Supporting Information

for

Bifunctional enhancement of photodetecting and photovoltaic parameters in graphene/porous-Si heterostructures by employing interfacial hexagonal boron nitride and bathocuproine back-surface passivation layer

Chan Wook Jang[1], Dong Hee Shin[2], and Suk-Ho Choi[1]*

[1]Department of Applied Physics, Institute of Natural Sciences, and Integrated Education Institute for Frontier Science and Technology (BK21 Four), Kyung Hee University, Yongin 17104, Korea

[2]Department of Physics, Andong National University, Andong, Gyeongbuk 36729, South Korea

*Corresponding author: sukho@khu.ac.kr

Table S1. Phtodetecting performance comparison of the TFSA-GR/h-BN/PSi/Si/BCP heterostructures with other self-powered GR/Si-heterojunction PDs previously-reported in literatures.

Device Structure	R (AW^{-1})	EQE (%)	D* (cm $Hz^{1/2}$ W^{-1})	Decay time (ms)	Ref
GR/h-BN/Si			2.8×10^{10}	1	17
GR/ZnO/Si	0.38	80	3.9×10^{13}	0.5	36
GR/Si	0.51			0.1	37
MoO_3-GR/Si		80	5.4×10^{12}		38
Bi-layer GR/Si	0.41		8×10^{12}	0.1	39
GR/Spiro-OMeTAD/Si	0.35		8.7×10^{10}	0.1	40
TFSA-GR/h-BN/PSi	0.55	88	2.6×10^{10}	0.03	This work
TFSA-GR/h-BN/PSi/BCP	0.58	88	1×10^{11}	0.04	

Table S2. Photovoltaic parameters of the TFSA-GR/PSi heterostructures without h-BN and BCP, with only h-BN, and with both layers

h-BN	BCP	V_{oc} (V)	J_{sc} (mA/cm^2)	FF (%)	PCE (%)
X	X	0.494	29.95	60.76	8.99
O	X	0.513	32.98	72.38	12.25
O	O	0.525	33.48	78.02	13.71

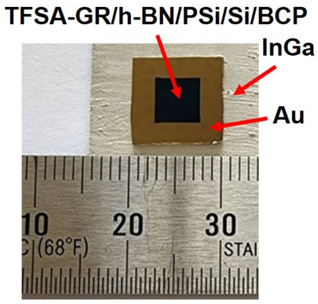

Fig. S1. Optical microscopic image of a typical TFSA-GR/h-BN/PSi/Si/BCP PD.

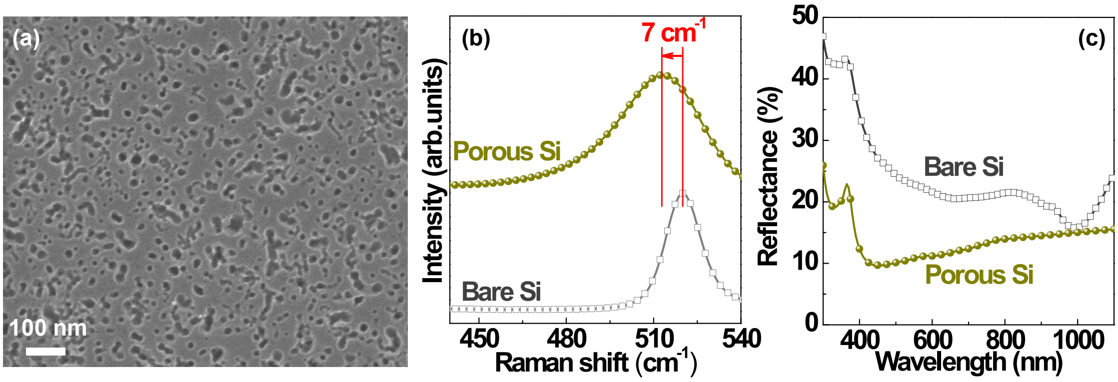

Fig. S2. FE-SEM images of (a) porous Si. (b) Raman and (c) reflectance spectra of bare Si and porous Si.

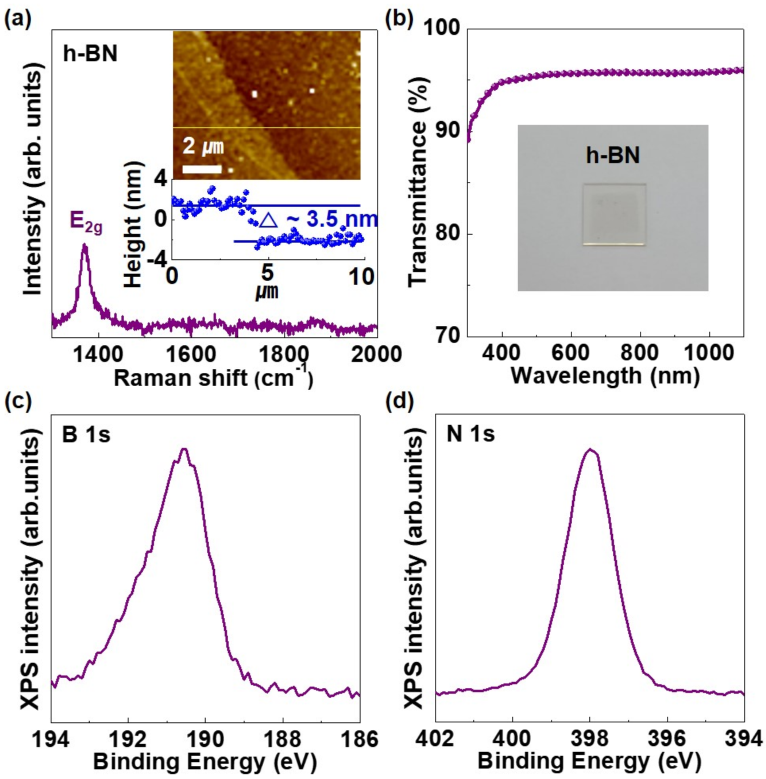

Fig. S3. (a) Raman spectrum of the h-BN layer. The inset shows the AFM topographic image and height profile of the h-BN sheet. (b) Transmittance of the h-BN sheet. The inset image shows the excellent transparency of the h-BN on quartz substrate. (c) and (d) XPS spectra of the h-BN sheet.

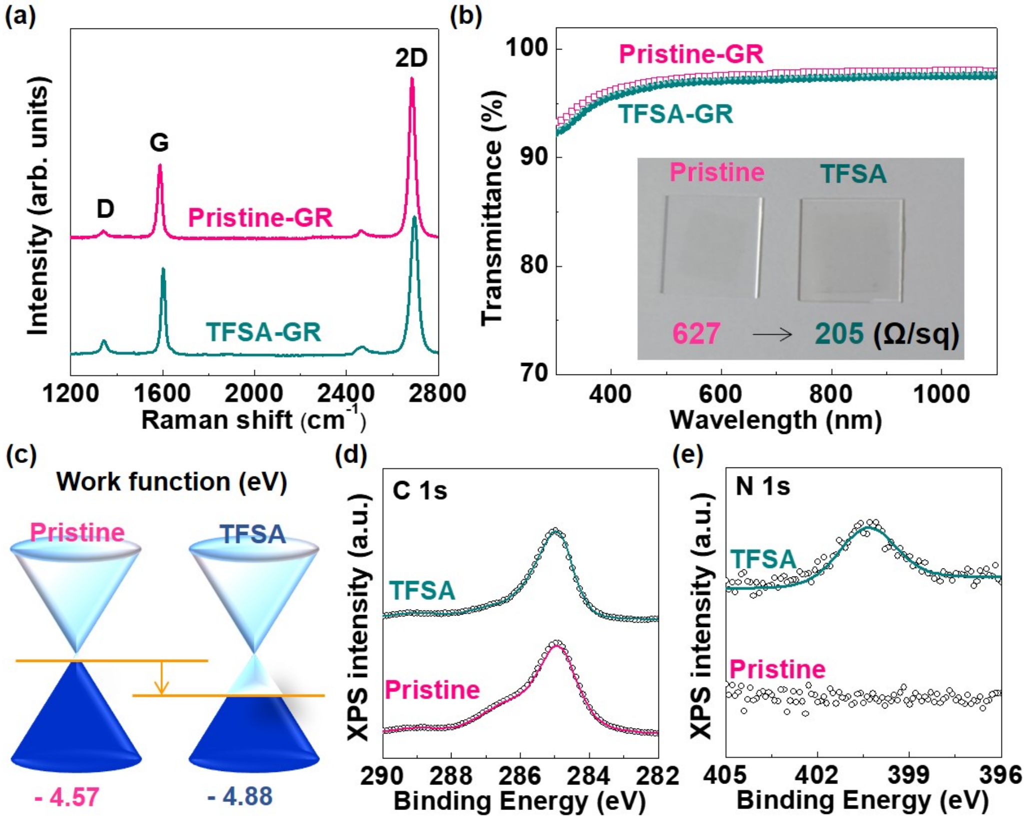

Fig. S4. (a) Raman spectra, (b) transmittance spectra, and (c) work function of the pristine GR and TFSA-GR. The inset in (b) shows the variation of the real image by the TFSA doping. (c) Work functions of pristine GR and TFSA-GR. (d) and (e) XPS spectra of the pristine GR and TFSA-GR.

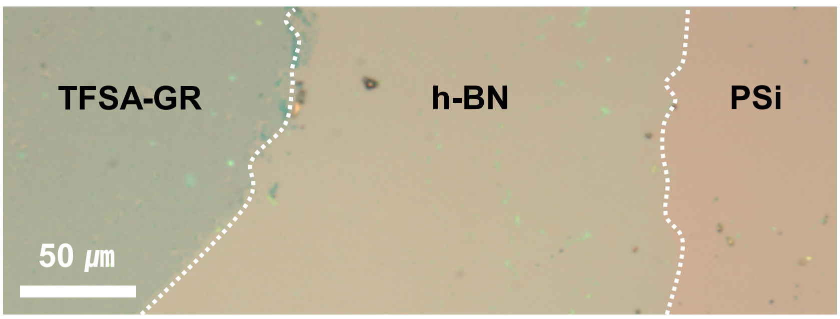

Fig. S5. **O**ptical microscopic image showing the uniformity of the 3 materials: TFSA-GR, h-BN, and PSi near the interfaces in the overlapped structure.

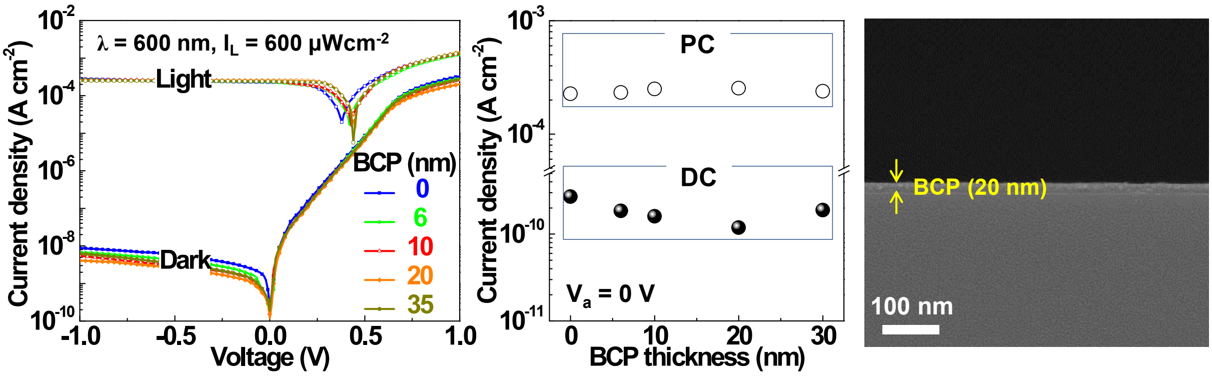

Fig. S6. Thickness-dependent photo/dark current density-voltage curves and PC/DC at 0 V for various BCP thicknesses, and a FE-SEM image showing the optimum thickness of the PD.

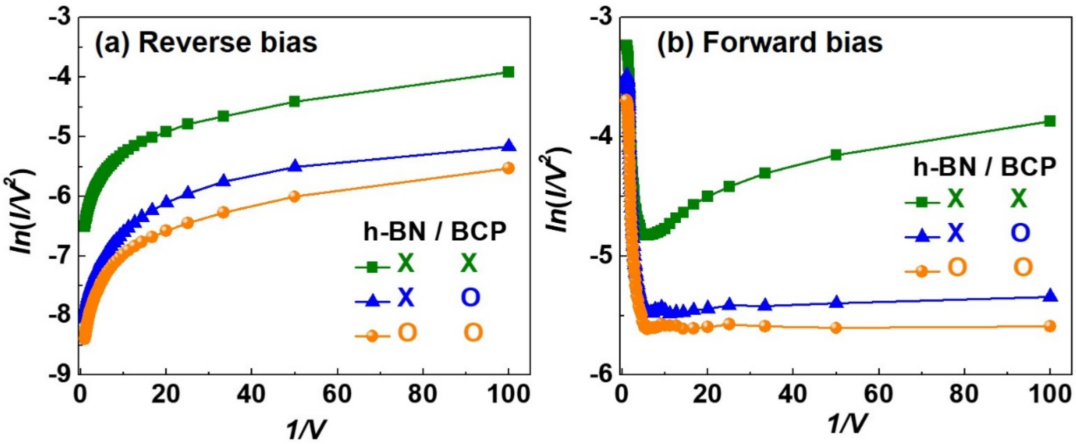

Fig. S7. Fowler-Nordheim-tunnelig plots (ln(I/V^2) vs 1/V) (a) under reverse bias and (b) under forward bias.

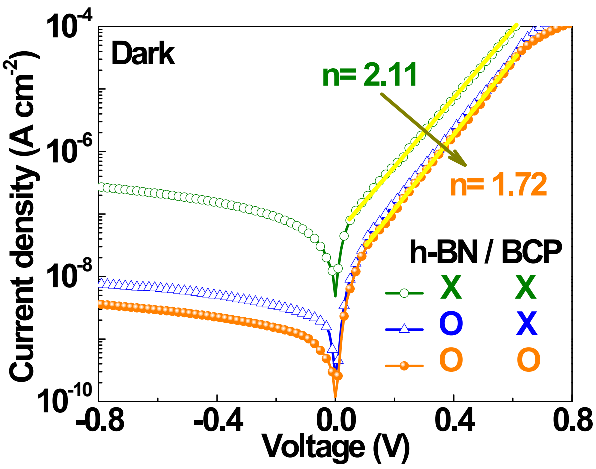

Fig. S8. Dark *J-V* curves of the heterostructures without h-BN and BCP, with only h-bN, and with both layers. The extracted ideality factors (n) are indicated.

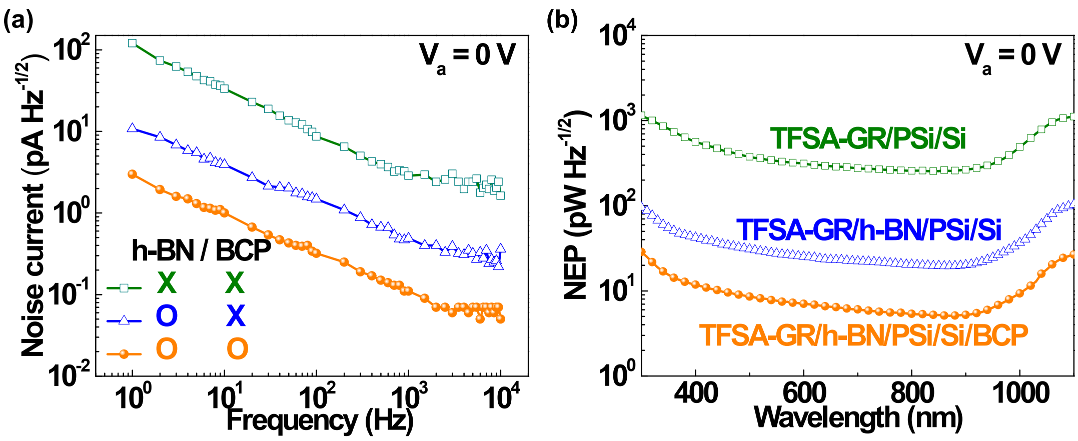

Fig. S9. (a) Frequency-dependent noise current and (b) λ -dependent NEP at zero bias for the heterostructures without h-BN and BCP, with only h-bN, and with both layers.

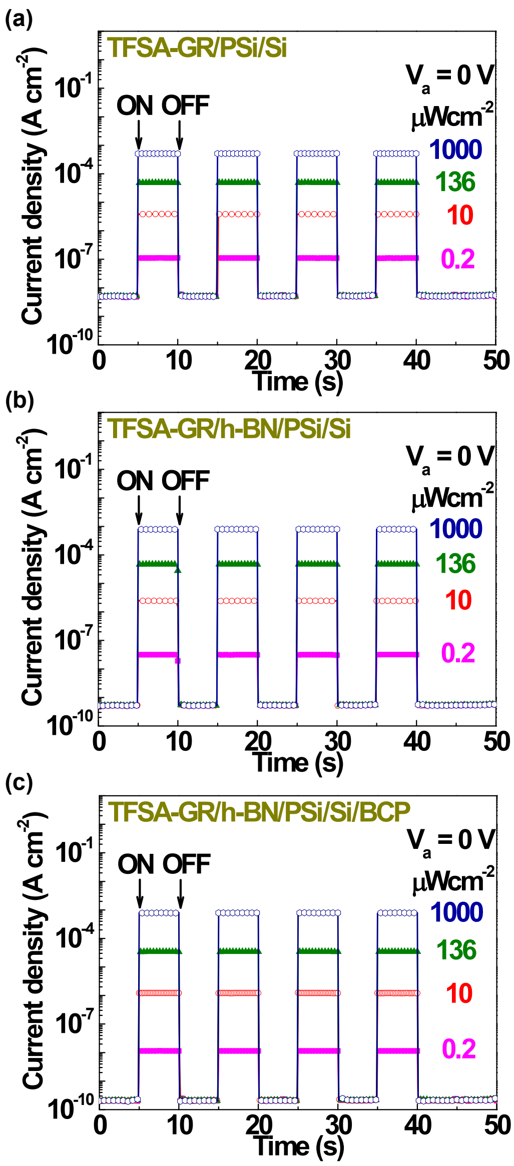

Fig. S10. Repetitive on/off switching current density characteristics for various lighting power for the heterostructures without h-BN and BCP, with only h-bN, and with both layers at zero bias.

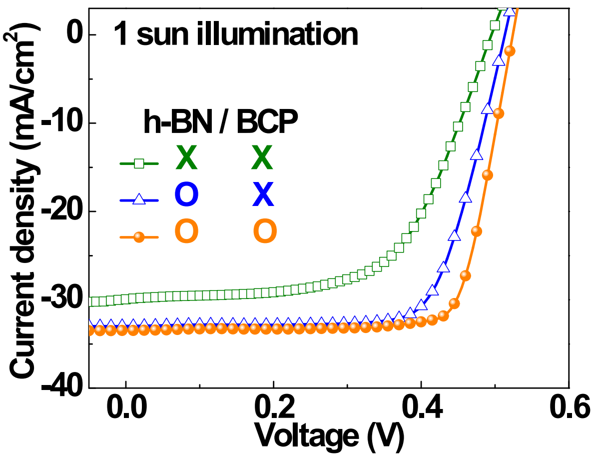

Fig. S11. *J-V* curves of the heterostructures without h-BN and BCP, with only h-BN, and with both layers under illumination of 1sun (100 mW cm^{-2} AM 1.5G) in air.

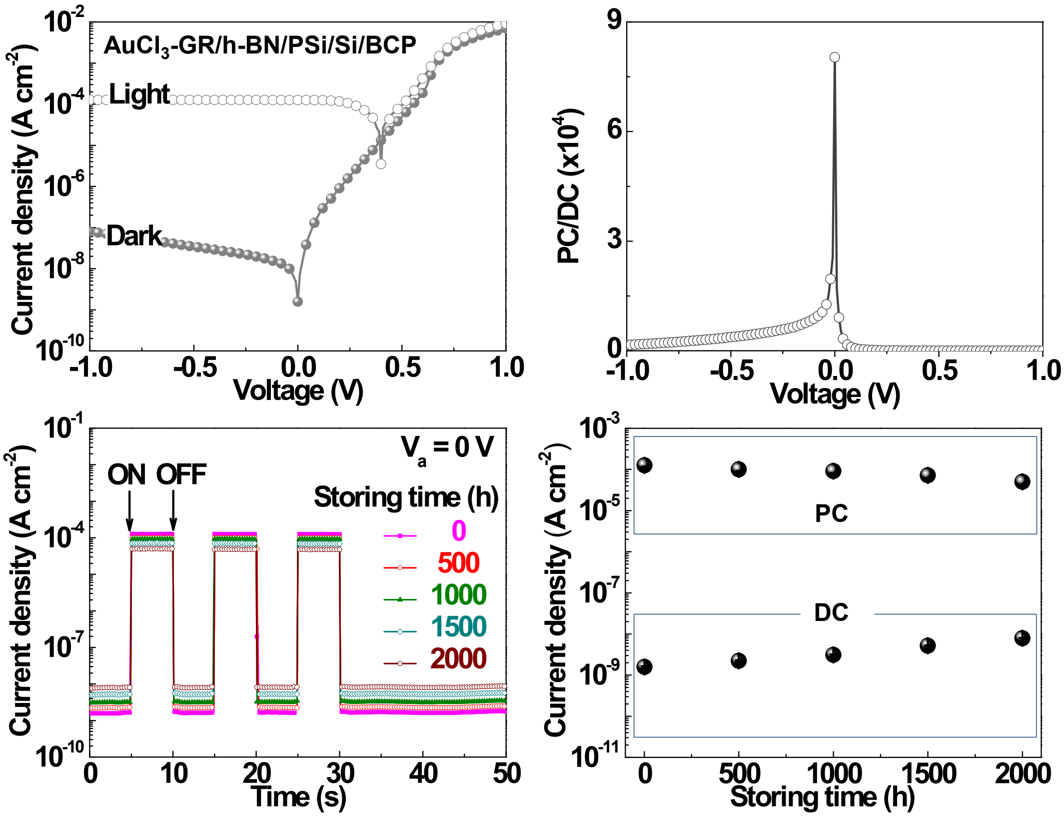

Fig. S12. Dark/photo current density-voltage curves, bias-dependent PC/DC ratio, temporal changes of the repeated on/off PC switching behaviors and the PC/DC under ambient conditions during 2000 h for a typical AuCl$_3$-GR/h-BN/PSi/Si/BCP.